SPH modelling and simulation of spherical particles interacting in a viscoelastic matrix

A. Vázquez-Quesada[1, a)] and M. Ellero[1, b)]
Zienkiewicz Centre for Computational Engineering (ZCCE), Swansea University, Bay Campus, Swansea SA1 8QQ, United Kingdom.
Tel.: +44 (1792) 295514

(Dated: Received: date / Accepted: date)

In this work, we extend the three-dimensional SPH non-colloidal particulate model previously developed for Newtonian suspending media in [Vázquez-Quesada, Ellero, J. Non-Newt. Fluid Mech., v. 233, pp. 3747, 2016] to viscoelastic matrices. For the solvent medium, the coarse-grained SPH viscoelastic formulation proposed in Ref. [Vázquez-Quesada, Ellero, Español, Phys. Rev. E, v.79, 056707, 2009] is adopted. Property of this particular set of equations is that they are entirely derived within the GENERIC formalism (General Equation for Non-equilibrium Reversible-Irreversible Coupling) and therefore enjoy automatically thermodynamic consistency. The viscoelastic model is derived through a physical specification of a conformation-tensor-dependent entropy function for the fluid particles. In the simple case of suspended Hookean dumbbells this delivers a specific SPH discretization of the Oldroyd-B constitutive equation. We validate the suspended particle model by studying the dynamics of a single and mutually interacting 'noncolloidal' rigid spheres under shear flow and in the presence of confinement. Numerical results agree well with available numerical and experimental data. It is straightforward to extend the particulate model to Brownian conditions and to more complex viscoelastic solvents.

Keywords: Smoothed Particle Hydrodynamics, viscoelasticity, non-colloidal particle suspension

I. INTRODUCTION

Understanding the dynamics of rigid particles interacting with complex viscoelastic matrices is important for the design of a wide range of products, including pneumatic tires in the automotive industry, gels/creams in the food/personal care industry as well as for biomedical applications.
Whereas simulation of particles suspended in a simple Newtonian matrix has often been proposed based on grid-based techniques - e.g. finite elements methods (FEM)[1], distributed Lagrange-multiplier-based (DLM)[2,3], smoothed profile methods (SPM)[4], finite volumes techniques[5] - and grid-off approaches - e.g. Stokesian Dynamics[6], Lattice Boltzmann methods[7,8], Dissipative Particle Dynamics[9–14], Smoothed Particle Hydrodynamics methods[15,16] - much less work has been devoted to particulate systems interacting with viscoelastic matrices. In particular, after the seminal grid-based simulation approaches in Refs.[17–19], novel arbitrary-Lagrangian-Eulerian (ALE) formulations have been proposed by Hulsen and coworkers which allowed improved calculations on moving domains[20]. Grid-based methods are able to capture accurately the dynamics of particles in viscoelastic media modelled by several constitutive equations - e.g Oldroyd-B, Maxwell, Giesekus, PTT, FENE-like etc. - and have been successfully applied to study the rotation of a sphere in a viscoelastic liquid subjected to shear flow[21], confinement effects on viscoelasticity-induced cross-stream particle migration[22,23], particle-interaction in a shear flow[19,24] and recently particle separation and sorting in microfludics devices[25]. Despite their great accuracy, these techniques are to date limited to small systems, i.e. in the order of hundreds of suspended discs in 2D[26] or few dozens of spheres in three-dimensional calculations[27]. In ALE approaches this is, from one hand, related to the need of frequent costly mesh generation when grid becomes too distorted during motion and, on the other one, to the request of local enrichment for numerical convergence in gaps between nearly touching particles. This problem makes therefore difficult to study the rheology of large particulate samples and/or to explore microstructural quantities requiring large statistics such as, for example, the radial distribution function. It should be noticed that recent unstructured finite volume methods for continuum viscoelastic flows have been coupled to moving domains using immersed boundary formulations[5] allowing parallel simulations of hundred spheres under dilute conditions[28].

The challenges in reproducing accurately and efficiently the dynamics of viscoelastic suspensions has driven the simultaneous development of alternative techniques. For example the Stokesian Dynamics method which, thanks to the absence of the explicit solvent calculation, allows for excellent algorithmic scaling[29], but it is typically applied to simple Newtonian suspending media. To the best of our knowledge, the only generalization to non-Newtonian media was proposed in Ref.[30] but the model was restricted to linear viscoelasticity. In the context of Lattice Boltzmann techniques, a recent hybrid two-dimensional approach

[a)] Electronic mail: A.Vazquez-Quesada@swansea.ac.uk
[b)] Electronic mail: M.Ellero@swansea.ac.uk

for particulate systems has been proposed in Ref.[31], where a LB-Giesekus model of the viscoelastic medium is combined with a solid-fluid interaction described by a smoothed profile method.
Among coarse-grained techniques for viscoelastic suspensions, it is worth mentioning the so-called responsive particle dynamics (RaPiD)[32], a particle-based off-lattice which can efficiently simulate various viscoelastic fluids ranging from polymeric dispersions to worm-like miscellar solutions. The method has been applied to study the alignment of particles under shearing[33,34], but is restricted to the Brownian regime, i.e. typically for submicron colloidal particles, so extensions to non-colloidal regime seems hard to obtain.

An alternative approach to describe viscoelastic media is represented by Smoothed Particle Hydrodynamics (SPH). The method has been traditionally introduced as a Lagrangian meshless discretization of viscoelastic partial differential equations, such as corotational Jaumann-Maxwell[35] or Upper-Convected Maxwell models[36].

Recently, a novel SPH viscoelastic formulation has been developed for mesoscopic Brownian regime by incorporating additional stochastic terms in the particle evolutions equations which satisfy exactly 2nd Law of Thermodynamics and the Fluctuation-Dissipation Theorem (FDT)[37,38]. Discrete enforcement of FDT is critical to model complex mesoscopic fluids[39] and it can be nicely obtained by casting the model into the so-called GENERIC formalism (General Equation for Non-equilibrium Reversible-Irreversible Coupling)[40]. In the limit where thermal fluctuations can be neglected, the coarse-grained model reduces to a very specific 'thermodynamic-consistent' SPH discretization of an Oldroyd-B constitutive equation. The resulting model has been successfully validated under transient and complex flows[37,41,42].
Beside formal aspects of thermodynamic consistency, SPH in particular - and particle methods in general - are defined in term of local pairwise interactions and therefore enjoy a high-degree of parallelization which make them suitable to use for HPC computations of large-scale particle systems. The SPH particle models presented here are implemented on the Parallel Particle Mesh library (PPM)[43], a Fortran 90 software layer between the Message Passing Interface (MPI) and Client Applications for simulations of physical systems using Particle-Mesh methods with optimal scaling performance.

In this work, we extend the SPH particulate models previously developed for Newtonian matrices[15,16] to viscoelastic matrices and validate them by studying the dynamics of a single and mutually interacting 'noncolloidal' spheres under confined shear flow. The deterministic non-Brownian SPH solvent model will be considered here, whereas its stochastic mesoscopic generalization[37] for a 'colloidal' particulate system will be presented in a future work. The scheme of the paper is the following one: in Sec. II, the SPH viscoelastic suspension model is presented. Sec. III is devoted to the numerical analysis, in particular we will consider four validation benchmarks: (i) bulk particle rotation; (ii) confinement effect on lateral particle migration, (iii) particle-pair interaction under shear flow and (iv) sedimentation of a many-particle system in a closed cavity. Finally, conclusion and future application of the methodology will be outlined in Sec. IV.

II. VISCOELASTIC SUSPENSION MODEL

In this section the details of the suspension model are presented, separately, for the viscoelastic solvent medium and for the suspended solid particles.

A. SPH viscoelastic solvent modelling

In this work we consider a coarse-grained fluid-particle model for a polymer solution originally proposed in Ref.[37,38]. Every particle is considered as a thermodynamic sub-system containing a given number of polymer molecules. The state of the fluid particle is characterized by a configuration tensor $\mathbf{c}$ that describes their underlying molecular elongation and orientation. The specification of very simple physical mechanisms inspired by the dynamics of single polymer molecules allows one, with the help of the GENERIC formalism, to derive the equations of motion for a set of fluid particles carrying polymer molecules in suspension which satisfy strictly thermodynamics consistency, i.e. 1st-2nd Law of Thermodynamics and FDT. For sake of clarity, in this section we provide a brief overview of the main discrete evolution equations (focusing on the deterministic limit) and discuss their interpretation in the context of constitutive viscoelastic models.
If we consider a set of fluid particles labelled by Latin indices $i, j = 1, .., N$, in the most general case, the GENERIC-derived ordinary differential equations for the positions, velocities and conformation tensor associated to each particles read

$$\dot{\mathbf{r}}_i = \mathbf{v}_i$$
$$m\dot{\mathbf{v}}_i = -\sum_j \left[\frac{P_i}{d_i^2} + \frac{P_j}{d_j^2}\right] W'_{ij}\mathbf{e}_{ij} + (D+2)\eta_s \sum_j \left[\frac{1}{d_i^2} + \frac{1}{d_j^2}\right] \frac{\mathbf{e}_{ij}\cdot\mathbf{v}_{ij}}{r_{ij}} W'_{ij}\mathbf{e}_{ij} + \sum_j \left[\frac{\boldsymbol{\tau}_i}{d_i^2} + \frac{\boldsymbol{\tau}_j}{d_j^2}\right]\cdot W'_{ij}\mathbf{e}_{ij}$$
$$\dot{\mathbf{c}}_i = \left(-\sum_j \frac{1}{d_j}\mathbf{v}_{ij}\,\mathbf{e}_{ij}W'_{ij}\right)\cdot\mathbf{c}_i + \mathbf{c}_i\cdot\left(-\sum_j \frac{1}{d_j}\mathbf{v}_{ij}\,\mathbf{e}_{ij}W'_{ij}\right)^T + \frac{2}{\lambda}d_i\,\boldsymbol{\sigma}_i\cdot\mathbf{c}_i \tag{1}$$

where m is the mass of each particle, D is the number of dimensions of the system, $\mathbf{v}_{ij} = \mathbf{v}_i - \mathbf{v}_j$ are the relative particle velocities, $W_{ij} = W(r_{ij} = |\mathbf{r}_i - \mathbf{r}_j|)$ a normalized smoothing kernel function, $W'_{ij} = \partial W(r)/\partial r|_{r=r_{ij}}$ its derivative and $\mathbf{e}_{ij} = \mathbf{r}_{ij}/r_{ij}$ the unit vector joining particle i and j. The number density on particle i is evaluated as a standard summation $d_i = \sum_j W_{ij}$, while the particle pressure P_i is computed by using an equation of state $P_i = c_s^2(\rho_i - \rho_0)$, c_s being the speed of sound, $\rho_i = md_i$ and ρ_0, respectively, the local and a reference mass density.

These set of Newton's equations for the particles can be interpreted as a specific Smoothed Particle Hydrodynamics (SPH) Lagrangian representation of the general momentum conservation with an additional evolution equations for the conformation tensor. In particular, the first two terms model the effect of the solvent, i.e. first summation in Eq. (1) represents the pressure gradient term, the second summation corresponds to the Laplacian of the velocity field (η_s is the solvent dynamic viscosity), whereas the third contribution can be interpreted as the divergence of a polymeric stress (we use here the convention of the sign opposite to the pressure). In the most general case, the latter reads

$$\boldsymbol{\tau}_i = -2d_i\,\boldsymbol{\sigma}_i\cdot\mathbf{c}_i \tag{2}$$

where λ is the polymer relaxation time and $\boldsymbol{\sigma}_i$ is a tensorial variable thermodynamically conjugated to $\mathbf{c}_i$, defined as

$$\boldsymbol{\sigma}_i = T\left(\frac{\partial S_p(\mathbf{c})}{\partial \mathbf{c}}\right)_i \tag{3}$$

where T is a constant temperature and $S_p(\mathbf{c})$ is the conformational-dependent entropy function. Expressions (1), (2) and (3) are of general validity as no assumption has been made yet on the specific force law of the polymer. Application of GENERIC ensures their thermodynamic consistency at the discrete level.

Polymer physics come into play in this model with a proper definition of $S_p(\mathbf{c})$. In the simplest case of a dilute suspension of Hookean dumbbells, this entropy reads[39]

$$S_p(\mathbf{c}) = k_B\frac{N_p}{2}\left(\mathrm{tr}[\mathbf{1} - \mathbf{c}] + \ln\det\mathbf{c}\right) \tag{4}$$

where k_B is the Boltzmann constant and N_p is the total number of dumbbells. In Ref.[37] we have shown that this specific choice leads to $\boldsymbol{\sigma}_i = \left(\mathbf{c}_i^{-1} - \mathbf{1}\right)$ and the resulting expression for the polymeric stress is

$$\boldsymbol{\tau}_i = \frac{\eta_p}{\lambda}\left(\mathbf{c}_i - \mathbf{1}\right) \tag{5}$$

where we have defined the polymeric viscosity as $\eta_p = N_p d_i k_B T\lambda$. Finally, the last term on the r.h.s. of the evolution equations (1) for $\mathbf{c}_i$ reduces to

$$\frac{2}{\lambda}d_i\,\boldsymbol{\sigma}_i\cdot\mathbf{c}_i = \frac{1}{\lambda}\left(\mathbf{1} - \mathbf{c}_i\right) \tag{6}$$

The resulting equations (1) correspond therefore to a very specific SPH discretization of the classical Oldroyd-B constitutive model for a dilute suspension of Hookean dumbbells. As shown in Ref.[37], this particular set of equations for the particles conserve local and total linear/angular momentum, energy (in the athermal case) and they are consistent with the 2nd Law of Thermodynamics.
Temporal integration of the above SPH equations for the solvent is performed with a second-order predictor-corrector scheme. For the weighting function W, the present work adopts a quintic spline kernel[44] with cutoff radius $r_{cut} = 4\,\mathrm{d}x$ ($\mathrm{d}x$ being the mean fluid particle separation)[45].

As mentioned above, the formulation given in Eq. (1) represents the deterministic continuum limit of a more general coarse-grained stochastic model obtained in the framework of GENERIC. It should be beard in mind that in such a derivation, no reference to a target PDEs (i.e. Oldroyd-B) is considered. The fact that a SPH discretization of an Oldroyd-B equation was finally recovered represents an 'a posteriori' proof of the consistency of the approach, as it is the expected result for Hookean dumbbells in suspension. Generalization to more complex polymeric models, such as finitely extensible nonlinear elastic springs, with the proper introduction of thermal fluctuations is straightforward[38]. In particular, coarse-grained thermodynamic consistent models can be constructed by physical specification of conformation-tensor-dependent entropy of the fluid particles appearing in Eq. (4), rather than by brute force discretization of existing continuum constitutive equations. For a more detailed discussion on the formal aspects of SPH and the link to GENERIC the reader is referred to Ref.[37].

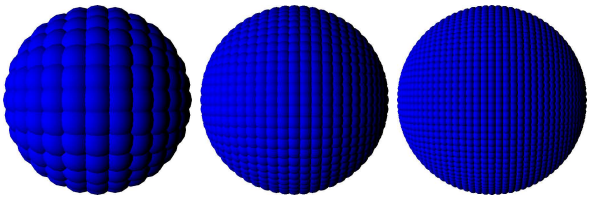

FIG. 1. Scheme of the location of the SPH boundary particles modelling a solid sphere. The depicted resolutions used in this work are $5, 10, 15$ SPH boundary particles per radius (left-middle-right) and correspond to a solid sphere described by approximately $520, 4180, 14130$ computational elements.

B. Solid particles: fluid-structure interaction

Solid inclusions of arbitrary shape can be modelled using boundary particles similar to fluid ones, located inside the solid region[46] (Fig. 1). Boundary particles interact with fluid particles by means of the same SPH forces described in Eq. (1). No-slip boundary condition at the liquid-solid interface is enforced during each interaction between fluid particle i and boundary particle j by assigning an artificial velocity to the boundary particle j, which satisfy zero interpolation at the interface[44]. The same approach can be also used to model any arbitrary external wall. Once all the forces acting on every boundary particle j belonging to a solid bead (labelled by Greek indexes $\alpha, \beta, ..$) are calculated, the total force $\boldsymbol{F}_\alpha^{\rm sph}$ and torque $\boldsymbol{T}_\alpha^{\rm sph}$ exerted by the surrounding fluid modelled by SPH can be obtained as

$$\boldsymbol{F}_\alpha^{\rm sph} = \sum_{j\in\alpha} \boldsymbol{F}_j, \qquad \boldsymbol{T}_\alpha^{\rm sph} = \sum_{j\in\alpha} (\boldsymbol{r_j} - \boldsymbol{R}_\alpha) \times \boldsymbol{F}_j \quad (7)$$

where $\boldsymbol{R}_\alpha$ is the center of mass of the solid bead α. When properly integrated, $\boldsymbol{F}_\alpha^{\rm sph}$ and $\boldsymbol{T}_\alpha^{\rm sph}$ allow to obtain the new linear velocity $\boldsymbol{V}_\alpha$, angular velocity $\boldsymbol{\Omega}_\alpha$ and position of the suspended solid bead. Positions of boundary particles inside α are finally updated according to a rigid body motion[47].

C. Short-range inter-particle forces

The present SPH model captures accurately the long range viscoelastic interactions between solid particles. As discussed in detail in Ref.[15,16,47] when two solid particles (e.g. α and β) get very close to each other, the hydrodynamic interactions (HIs) mediated by the SPH fluid are poorly represented and need to be corrected.

In Ref.[15,16,47] an analytical solution has been considered for the pairwise short-range HIs obtained in the limit of small sphere's separation and superimposed it to the far-field multi-body SPH HIs. In the case of a Newtonian fluid, the normal and tangential lubrication forces acting between the spheres read:[48].

$$\begin{aligned} \boldsymbol{F}_{\alpha\beta}^{{\rm lub},n}(s \le s_c^n) &= f_{\alpha\beta}(s)\boldsymbol{V}_{\alpha\beta}\cdot\boldsymbol{e}_{\alpha\beta}\boldsymbol{e}_{\alpha\beta} \\ \boldsymbol{F}_{\alpha\beta}^{{\rm lub},t}(s \le s_c^t) &= g_{\alpha\beta}(s)\boldsymbol{V}_{\alpha\beta}\cdot(\boldsymbol{1} - \boldsymbol{e}_{\alpha\beta}\boldsymbol{e}_{\alpha\beta}) \end{aligned} \quad (8)$$

where $\boldsymbol{e}_{\alpha\beta} = \boldsymbol{R}_{\alpha\beta}/R_{\alpha\beta}$ is the vector joining the centers of mass of solid particles α and β, $\boldsymbol{V}_{\alpha\beta}$ is their relative velocity and $s = R_{\alpha\beta} - (a_\alpha + a_\beta)$ is the distance in the gap between sphere-sphere surfaces and a_α and a_β are the sphere's radii. Normal/tangential lubrication is switched only at small separation distances s_c^n, s_c^t which depend on the particle resolution dx. Full details about the lubrication scheme as well as the expression for the scalar functions $f_{\alpha\beta}(s)$ and $g_{\alpha\beta}(s)$ are given in Ref.[15,16,47]. An accurate semi-implicit splitting scheme[49] for the time integration of the short-range lubrication forces presented in Ref.[15] is used. The novel strategy avoids a costly full matrix inversion by generating a series of small linear systems which can be solved analytically, reducing drastically the CPU time to simulate dense systems.

A discussion on this choice of short-range interparticle lubrication is in order. In Ref.[15,16,47] it was shown that this contribution captures accurately the effect of the "unresolved" squeezing flow in the gap s between two approaching particles when $s \ll a$. In the situation considered in this work, the suspending medium is non-Newtonian, i.e. viscoelastic, and mathematically speaking, the incorporation of Newtonian lubrication would be inconsistent with the far-field hydrodynamic interactions. To solve this problem, some authors adopt the approach of grid refinement in the gap between approaching suspended spheres[19,20,26,27]. This bypasses the problem of introducing a "model" for short-range interactions as the fluid should be "everywhere resolved" according to the given constitutive equations. We should point out that this approach, although being mathematically consistent, might not be fully compliant with the underlying physics of the fluid. In fact, validity of the any continuum model relies on assumption of sufficient regularity of the fields describing the fluid. This is generally obtained by requiring the existence of a scale separation[50], i.e. at least $\mathcal{O}(10)$, between the typical size of the microscopic constituents (atoms, molecules etc.) and the physical size of the 'minimal' portion of fluid (grid cell, volume etc.) used in the discretization of the PDEs . Now, whereas for simple fluids such as water, this condition is manifestly satisfied down to extremely small scales (size of a water molecule is $\approx$ 0.2nm) and justifies the application of Stokes equations (and relative lubrication solution) to nanometer scales, the same is not necessarily true for high molecular weight polymeric fluids such the Boger matrices targeted here. In Boger liquids[51] the matrix is typically formed from highly-viscous Newtonian fluids, such as corn-syrup or glycerine/water mixtures (to match bead density), in which a very small amount (0.03 % or smaller) of polyacryliacid (PAA) at high molecular weight (5×10^6 g/mol) is dissolved. According to manufacturer, PAA

molecules are characterized by a typical gyration radius (under no flow condition) $R_g \approx 100$nm, whereas at very high shear rates a coil-stretch transition might occur, leading to physical size exceeding μm. It is clear that any continuum description for these fluids is questionable on scale smaller than, say, few microns at best. In the case of non-colloidal spheres with typical radius $\approx 40\mu$m, for example, this would lead to a failure of continuum hypothesis on scales of the order of 10% of the particle radius. So, although it is mathematically correct to search for a numerically converged-solution of the PDEs, it might be questionable to push its validity in the very narrow gaps occurring between nearly touching particles.
In this work, we consider the short-range interparticle lubrication model based on the Stokes expression with Oldroyd-B viscosity, therefore in this approximation we merge a far-field viscoelastic description of HIs with a short-range Newtonian behaviour. Appropriateness of this approximation can be assessed a posteriori by exploring the particle dynamics under different flow conditions, which is what we do in Sec. 3.

Finally, beside short-range lubrication forces, an additional repulsive force acting between solid particles is introduced to mimic particle's surface roughness or other short-range interactions (e.g. electrostatic) which prevents artificial overlap[15,16,47]. It is customary to use for this force the expression[52,53].

$$\boldsymbol{F}^{\rm rep}_{\alpha\beta} = F^{\rm rep}\frac{\tau e^{-\tau s}}{1-e^{-\tau s}}\boldsymbol{e}_{\alpha\beta} \qquad (9)$$

where τ^{-1} determines the interaction range and $F^{\rm rep}$ its magnitude. Typically values for nearly hard-spheres are $\tau^{-1} = 0.001a - 0.05a$ and $F^{\rm rep} = 2.115$ (see Ref.[16]). Larger values of τ^{-1} describe soft spheres with finite repulsion range.

III. NUMERICAL RESULTS

In this section we present results of the simulation of the suspension model for rigid particles under shear and in presence of confinement. We present first validation tests of the model for a single particle under rotation in a shear flow (Sec. III A), particle migration under confined conditions (Sec. III B), two-particles interaction in a shear flow (Sec. III C) and sedimentation of a many-particle system in a closed cavity (Sec. III D).

A. Rotating sphere in a viscoelastic medium

In order to validate the model, the case of a freely rotating non-Brownian, buoyancy-free sphere in a constant shear rate flow is considered first. A sphere of radius $a = 1$ is confined symmetrically between two planar walls moving at velocities $\pm V$, generating a shear rate

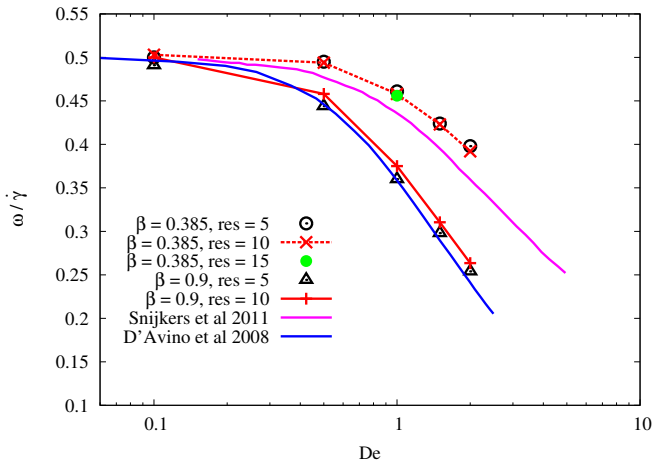

FIG. 2. Angular rotation of a sphere in a viscoelastic medium undergoing shear flow. Comparison of the simulations with literature.

$\dot\gamma = 2V/L$, with L being the gap between the plates. Periodic boundary conditions are imposed in the remaining directions.
The viscoelastic parameter $\beta = \eta_p/\eta_t$ (with $\eta_t = \eta_p + \eta_s$) characterizes the amount of liquid elasticity, being zero for a Newtonian fluid and one for a purely elastic fluid, i.e. Upper-Convected Maxwell model. We consider here two different values: $\beta = 0.385$ and 0.9. Simulations have been performed by maintaining a constant solvent viscosity $\eta_s = 15.55$ and adjusting η_p in order to achieve the desired β value. To characterize the elasticity regime the Deborah number is used, which is defined as $\mathrm{De} = \dot\gamma\lambda$, with λ being the characteristic elastic time of the fluid. The size of the simulation box is $L_x = L_y = L_z = 10a$ chosen to minimize periodicity and confinement effects. Box size effects have been assessed by running simulations at the largest De with $L_x \times L_y \times L_z = 20a \times 10a \times 20a$ without producing deviations in the results. To check numerical convergence, two resolutions are considered first, namely res= 5 SPH particles (see sketch Fig. 1) and res= 10 SPH particles per solid particle radius. This corresponds, respectively, to a total number of simulated SPH particles $N \approx 150,000$ and $N \approx 1,100,000$, whereas the numbers of SPH boundary particles per solid bead are approximately 520 and 4,180. In one case we have performed the simulation at even higher resolution, i.e. res= 15, to check the convergence. This last case corresponds to a total number of $N \approx 3,600,000$ SPH particles with approximately 14,130 SPH boundary particles per solid bead.

The total viscosity is, respectively $\eta_t = 25.28$ ($\beta = 0.385$) and $\eta_t = 155.55$ ($\beta = 0.9$). The imposed shear rate is varied in the range $\dot\gamma = 0.018 - 0.355$, producing a maximum particle Reynolds number $\mathrm{Re} = \rho a^2\dot\gamma/\eta_t = 0.014 \ll 1$. Speed of sound is chosen $c_s = 140$, leading to a Mach number $\mathrm{Ma} = V/c_s = 0.013 \ll 1$, therefore an approximately

incompressible inertia-less flow is modelled.
Before starting the simulation, the square lattice defining the initial positions of the SPH fluid particles has been randomized to avoid spurious fluctuations. The simulations are compared against the numerical and theoretical results from literature. In particular, results of simulation done with an Oldroyd-B fluid from Snijkers et al in[54] as well as with a Maxwell fluid by D'Avino et al[21] are considered as reference.

Comparison is reported in figure 2, where numerical convergence and overall good agreement is obtained with SPH up to De = 2. The solid particle rotates in the shearing plane with a rate ω dependent on the applied shear rate, delivering the classical result $\omega = \dot{\gamma}/2$ in the Newtonian limit (De $\to$ 0) and a reduction of the rotation rate with increasing elasticity, in agreement with simulations[21,54] and experimental results with Boger liquids[55]. The present results show also that 5 SPH boundary particles per radius is a sufficient resolution to capture accurately the dynamics of a single sphere undergoing a shear flow in the regime of De investigated.

B. Lateral particle migration

As a second validation test, we check the dynamics of a particle undergoing a shear flow in presence of planar confinement. Upper/lower plates are translated with constant velocities $\pm V$ generating a shear flow $\dot{\gamma} = 0.5$. As in the previous case $\beta = \eta_p/\eta_t = 0.9$ and the Reynolds and Mach numbers are small, i.e. Re $\approx 0.003 \ll 1$ and Ma $\approx 0.04 \ll 1$. Size of simulation box is now $L_x = 20a, L_y = 10a, L_z = 10a$, with blockage ratio $L_z/a = 10$. Modelling the solid spheres with res=5 boundary particles corresponds to $N = 300,000$ total SPH computational elements, whereas res=10 corresponds to $N = 2,200,000$. When initially located on the middle plane (as in the previous case), the particle just rotates. However, when displaced from the symmetry plane, lateral migration along the gradient direction occurs. The first evidence of cross-streamline migration in planar shear flow was given in Ref.[56], whereas recent simulations[22,23] and experiments with Boger liquids[57] indicate that fluid viscoelasticity drives particles towards the closest wall, as opposed to the common phenomenon of lateral inertia-driven migration towards middle plane predicted in Newtonian fluids[58].

As discussed in Ref.[59] in the viscoelastic case, it is the presence of confinement that leads to an asymmetric shear rate distribution around the particle (when placed off the midgap) resulting in a normal stress imbalance responsible for the net migration force.

In the Fig. 3 particle migration at De = 1 is shown for different initial positions. Results compare well with previous numerical simulations at same Deborah number, β and blockage ratio reported in Ref.[23]. Lateral migration

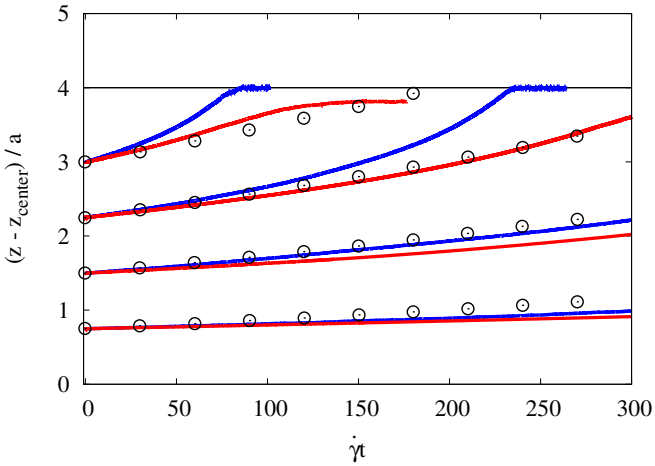

FIG. 3. Lateral migration. Particle position vs time for De = 1: res=5 (blue line), res=10 (red line). Results of[57] have been also reported (○).

is small near the middle plane (where the configuration is just weakly asymmetric), being enhanced towards the walls. Convergence of the results is checked for all trajectories. Whereas the bulk trajectories shows minor cumulative differences for a resolution change, the two upper trajectories fastly approaching the wall (i.e. lateral initial position $(z-z_c)/a = 3, 2.3$) deserve some discussion.. It is clear that the two-resolution dynamics still converge numerically for particle trajectories far from the wall and agree well with previous results[23]. However, for the upper blue trajectory when the particle gets close to the walls, i.e. for $(z - z_c)/a \geq 3.5$ disagreement arises. This case corresponds to a typical wall/sphere-surface separation $s \approx 0.5a$ which at low resolution considered (res=5, blue line) is $\approx 2.5\mathrm{d}x$, with dx being the mean SPH particle spacing. Due to the fixed low resolution used in this case, it is not surprising that viscoelastic wall-induced interactions mediated by the liquid are not accurately captured for gaps in the order of few SPH particle spacing. By increasing the resolution (res=10, red line), convergence of the particle trajectory is achieved to smaller wall-distances and agreement with results of Ref.[23] re-established.
It should be noted that the deviations shown in Fig. 3 (closest wall trajectory) correspond to an erroneous cumulative near-wall lateral displacements smaller than $0.5a$ (at res=5) and $0.1a$ (at res=10) for overall longitudinal displacements of the sphere in the flow direction of order of $40L_x \approx 800a$, so the relative displacement error is very small.
Some snapshots of the lateral particle migration and corresponding trace of conformation tensor Tr($\mathbf{c}$) are depicted in Fig. 4. This scalar field corresponds to the local state of polymer elongation, being equal to 3 under equilibrium isotropic conditions.

It should be noted that in our simulations - even at the largest resolution (red line Fig. 3) - the near-wall

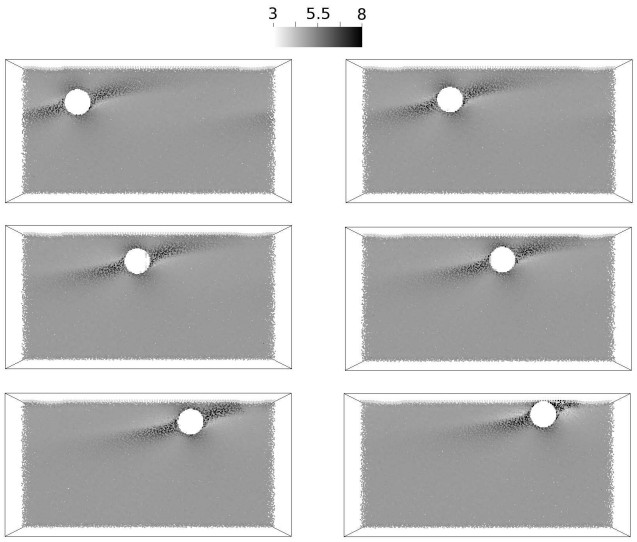

FIG. 4. Viscoelasticity-induced lateral migration. De = 1. Trajectory corresponding to initial lateral position $(z - z_c)/a = 2.3$. 2D-projection of the $\mathrm{Tr}(\mathbf{c})$ is taken in the middle shearing plane. Snapshots correspond to strains $\dot{\gamma}t = 8.6, 60.0, 128.6, 162.8, 194.3, 237.1$.

lateral migration is slightly over-estimated compared to the results reported in Ref.[23]. As discussed above, this can be related to a resolution effect in the gap, where a small number of SPH particles results in under-estimated bead-wall HIs. Another possible explanation is that in Ref.[23] a slightly shear-thinning Giesekus model was used with mobility parameter $\alpha = 0.2$; it is known that normal stress-difference are smaller for a Giesekus compared to an Oldroyd-B fluid, so if lateral migration is generated by an imbalance on normal stresses around the particles, bigger asymmetries and resulting enhanced migration might be expected here. This is also consistent with the recent two-dimensional simulations of Choi et al.[20] where a sensitivity analysis of the particle lateral migration as a function of the mobility parameter α in the Giesekus model was made. It was shown by the authors that by increasing α, the radial migration becomes slower. Since the Oldroyd-B model is recovered from the Giesekus model in the limit $\alpha \to 0$, the previous results of Ref.[20] explain qualitatively the slightly increased migration reported here.

C. Two-particles trajectories in a shear flow

In this section, the trajectories of two solid spheres approaching each other under uniform shear flow (Fig. 5, top) are investigated. The Newtonian case delivers passing trajectories with fore-aft symmetry which have been already discussed in Ref.[16], where excellent agreement compared with the analytical solutions of Batchelor[60] was found. We report here the analogous situation for a

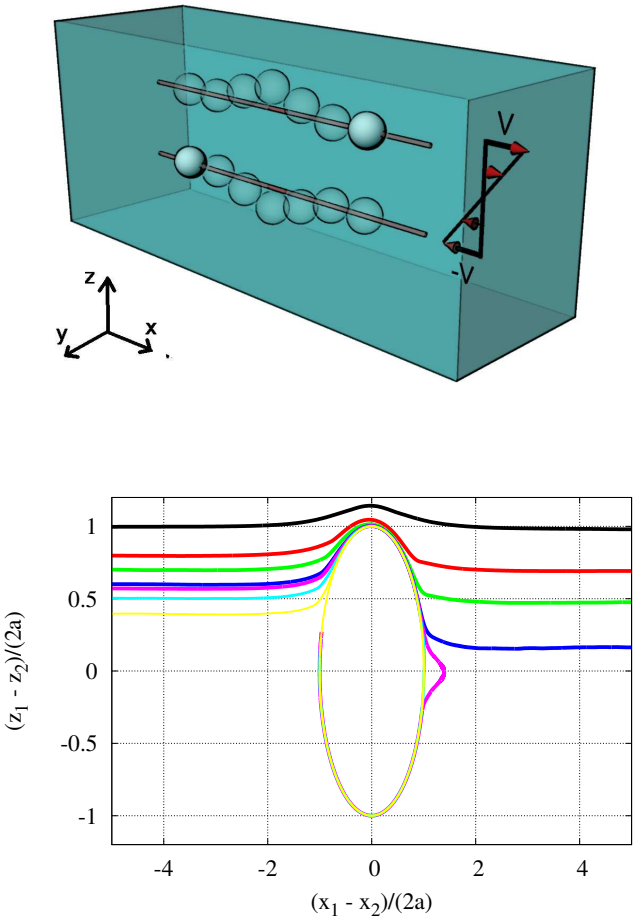

FIG. 5. Top: sketch of the simulations of two particles rotating and approaching each other in a uniform shear flow. Bottom: particle trajectories at De = 0.5.

viscoelastic Oldroyd-B matrix. Both spheres have identical radii $a = 1$ and simulation box size is $L_x = 20a, L_y = 10a, L_z = 20a$. A fluid with $\beta = 0.5$ is considered for a Deborah number De = 0.5, comparable to that used in Ref.[19,24]. As in the previous section the choice of viscosity, density, shear rate and speed of sound - which are taken respectively as $\eta_t = 31.11$, $\rho = 1$, $\dot{\gamma} = 0.5$ and $c = 70$ - ensures that the Reynolds and Mach numbers are much smaller than 1.

Results are presented in Fig. 5(bottom), where particles interact only 'hydrodynamically', i.e. no repulsion is considered ($F^{\mathrm{rep}} = 0$). Whereas for inertia-less Newtonian liquid (with hydrodynamic interparticle interactions only, i.e. no repulsion) the dynamics is perfectly reversible due to the time-invariance of the Stokes equations, viscoelasticity (with associated elastic memory) introduces a break-down of symmetry, so irreversibility and fore-aft asymmetries in the trajectories are expected.

In particular, a number of numerical studies with Oldroyd-B models show that the particles approach each

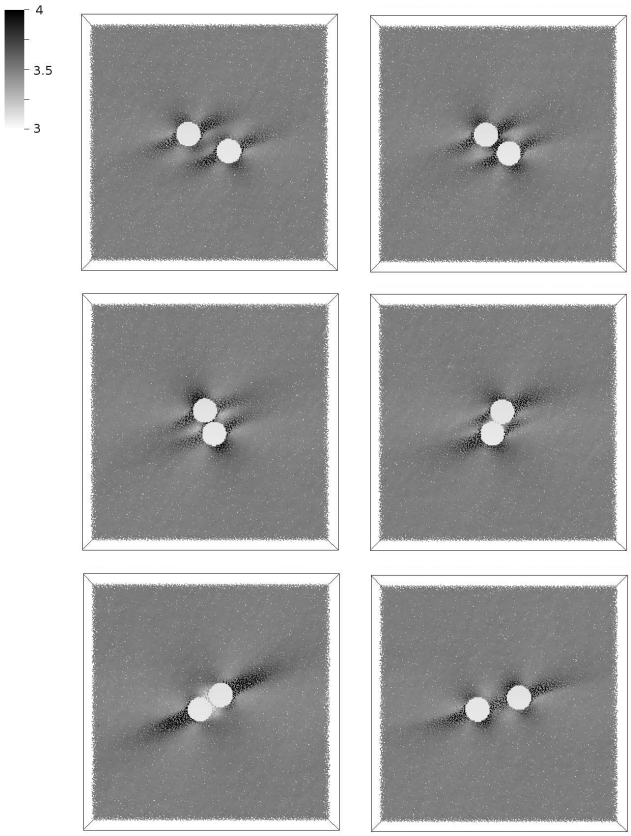

FIG. 6. Passing trajectory corresponding to an initial lateral separation $\tilde{z} = (z_1 - z_2)/2a = 0.7$, De $= 0.5$, $\beta = 0.5$. 2D-projection of the Tr(**c**) is taken in the middle shearing plane. Snapshots correspond to strains $\dot{\gamma}t = 4.86, 6.0, 6.86, 8.0, 9.14, 11.14$.

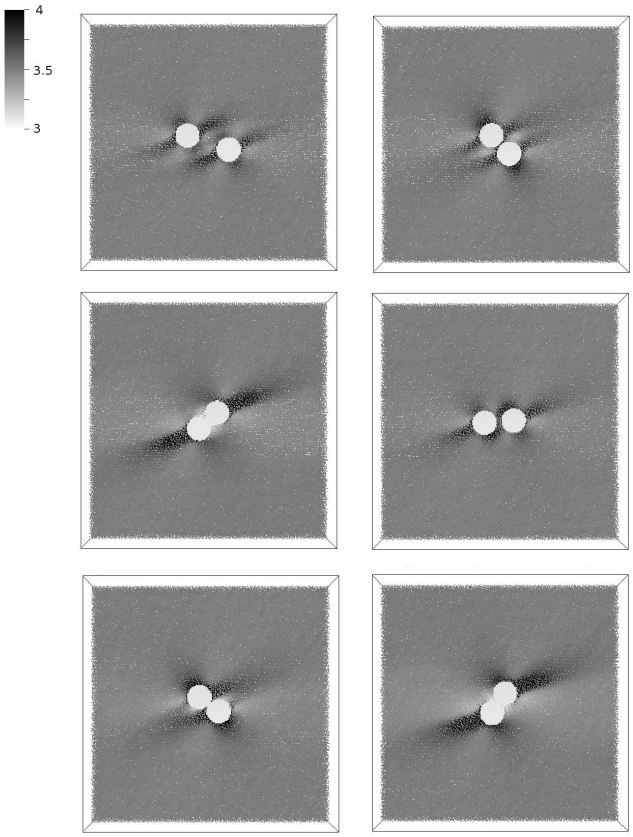

FIG. 7. Tumbling trajectory corresponding to an initial lateral separation $\tilde{z} = (z_1 - z_2)/2a = 0.575$, De $= 0.5$, $\beta = 0.5$. 2D-projection of the Tr(**c**) is taken in the middle shearing plane. Snapshots correspond to strains $\dot{\gamma}t = 5.91, 7.91, 11.34, 16.77, 34.77, 40.2$.

other along curvilinear paths (as in the Newtonian case) but, for close encounters, whereas at low De they separate (passing motion), for increasing Deborah number they start rotating permanently as a rigid dumbbell (tumbling motion)[19,24]. Remarkably, no tumbling motion has ever been observed in experiments with Boger liquids[61]. Moreover, experiments report asymmetric and strongly radially shifted trajectory (departing them) when shear-thinning polymer matrices are considered, whereas only minor inward shift (approaching them) is observed for constant viscosity Boger fluids. The latter situation is closer to the Oldroyd-B constitutive models considered in this work.
We have checked that for two particles initially placed far apart ($x_1 = 5a$, $x_2 = 15a$), Newtonian trajectories are passing symmetric for each initial lateral separation.

In the viscoelastic case, at large initial interparticle lateral separations, trajectories do still show passing characteristics with no visible asymmetry (Fig. 5 bottom: black line). However, for initial lateral separations $\tilde{z} = (z_1 - z_2)/2a \leq 0.8$ (red line) trajectories start to exhibit a mild inward shift, forcing post-colliding particles towards the middle plane and reducing $\tilde{z}$ further, i.e. a clustering tendency. This is in qualitative agreement with previous two-dimensional simulations with the Oldroyd-B model[19]. In that work the authors report tumbling for an initial lateral coordinate (following the definition of this work), $\tilde{z} = 0.064/0.24 \approx 0.26$. In order to explore a possible limiting tumbling behaviour we have launched a set of simulations with smaller initial lateral displacements. Size of the simulation box is chosen sufficiently large to avoid periodicity effects. From Fig. 5 (bottom) it is clear that for $\tilde{z} \approx 0.6$ (blue line) the trajectory undergoes a significant inward shift but no tumbling is observed yet. $\tilde{z}$ needs to decrease down to ≈ 0.57 (purple line) to lead to a kissing-tumbling dynamics (see limiting closed trajectory).

In order to explore the nature of the asymmetric passing and tumbling dynamics, we show next the trace of the polymer conformation tensor **c** at different stages.

2D projections of the full 3D fields are considered along the middle sharing plane intersecting the particle's centres. Fig. 6 corresponds to a passing dynamics for initial $\tilde{z} = 0.7$ (green trajectory in Fig. 5). Dark areas in the grey scale plot correspond to large values of Tr(**c**) and pronounced elongational flows. The three snapshots top/bottom correspond to times symmetrically taken before/after the "contact" defined as the configuration with minimal inter-particle distance (corresponding to the particles aligned along the vertical axis). Asymmetry in the Tr(**c**) is visible which leads to the fore-aft asymmetric trajectory shown in Fig. (5) and inward shift.

Fig. 7 shows the evolution of Tr(**c**) for the tumbling dynamics corresponding to an initial lateral displacement $\tilde{z} = 0.575$ (purple trajectory in Fig. 5). Similar to the 2D results presented in Ref.[19], the particles tumble around each other (snapshots 2,3), then separate temporarily (4) before recoiling and tumbling again (5,6). Note also the similarity in the distribution of the trace of the conformation tensor at different stages of the process (2D projection Fig. 7) compared with Ref.[19] where the Oldroyd-B equation was fully resolved in the interstial gap between two particles. The present results justify also the use of the lubrication model described in Sec.II C.

It should be remarked that this permanent rotational phenomenon was not observed in recent simulations of particle interacting under a "confined" situation[20,24], where instead a transition between passing/tumbling and returning motion was observed. It should be pointed out that in those works strong confinement was considered ($L_z = 10a$), whereas in the present study a very weak confinement was chosen ($L_z = 20a$) to minimize long-range particle-wall interactions and reproduce an approximate bulk behaviour.

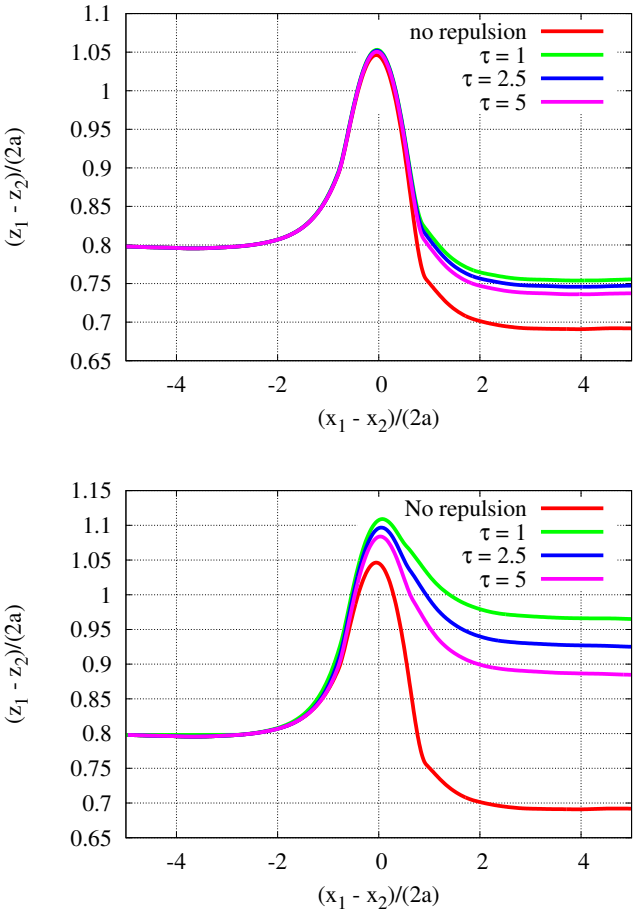

FIG. 8. Trajectories of two particles approaching each other in a uniform shear flow at De = 0.5 with the repulsion force (9). Different values of τ are taken for $F^{\rm rep} = 2.115$ (top) and $F^{\rm rep} = 21.15$ (bottom).

Note that in experiments[61] no tumbling is observed down to $\tilde{z} \approx 0.175$ which is inconsistent with the results reported here and in Ref.[19]. In order to see tumbling, possibly smaller initial lateral separation $\tilde{z}$ might need to be considered in experiments.

Another possibility is the breakdown of viscoelastic hydrodynamic interactions at very small interparticle distance (e.g. due to particle surface's roughness or other non-hydrodynamic repulsion forces).

In order to explore this effect, we study next the influence of the repulsion force (9) on the trajectories of two particles interacting in a shear flow, in particular we change the magnitude parameter ($F^{\rm rep}$) and the range parameter (τ). To this end, the trajectory with an initial lateral displacement $\tilde{z} = 0.8$ (red line in Fig. 5) is considered. Results have been drawn in Fig. 8. Different values of τ have been taken for two different values of $F^{\rm rep}$: $F^{\rm rep} = 2.115$ (top) and $F^{\rm rep} = 21.15$ (bottom). It is clear that the repulsion force reduces significantly the inward shift observed in the trajectories and it is even able to reverse it (from inward-shift to outward shift) for values of $F^{\rm rep}$ sufficently large (see $F^{\rm rep} = 21.15$ case). Repulsion has a counter-effect with respect to viscoelasticity, inducing radial departure of post-colloiding particles. It might be therefore expected that balance between the two effects can be obtained under a specific choice of parameters. As a matter of fact, one should notice the green line (Fig. 5 top) where a 'quasi-sysmmetric' trajectory is obtained for $\tau = 1$.

D. Many-particles sedimentation

In order to demonstrate the capability of the present model, in this section we present the result of a sedimentation of many interacting spheres in a closed box under quiescient initial conditions. The length of the box is $L_x \times L_y \times L_z = 16a \times 16a \times 64a$ and it is bounded by solid walls in every direction. The gravity force acts in the $z-$direction and is modelled by applying an external constant force on the solid particles, leading to an effective

sedimentation force $F_b = 161$. Initially $5^3 = 125$ spheres are located on a grid at the top part of the box. Resolution was taken res=5 (see Fig.1) and $N = 2,048,000$ SPH particles. Solvent mass density was $\rho = 1$, solvent viscosity $\eta_s = 5.20$, total viscosity $\eta_t = 8.46$, in such a way that $\beta = \eta_p/\eta_t = 0.385$. Relaxation time was $\lambda = 0.94$ and the speed of sound was $c_s = 50$. The corresponding dimensionless numbers were $\mathrm{Re} = \rho a V/\eta_t = 0.5$, $\mathrm{Ma} = V/c_S = 0.0846$ and $\mathrm{De} = \lambda V/(L_x/2) = 0.5$ where $V = 4.3$ was the average limiting particle sedimentation velocity.

With relation to the interparticle repulsion (Eq. (9)), different parameters of the force have been considered to check the deviations in the dynamics. Change of τ in the range $[20-1000]$ produces minor changes in the dynamics of the sedimenting particles which behave as nearly-hard spheres. To obtain a markedly changed dynamic behavior, in Fig. 9 we have considered two simulations with the same $F^{\mathrm{rep}} = 100.0$ and, respectively $\tau = 20.0, 1.0$. For $\tau = 20.0$ (nearly hard-sphere model: Fig. 9-top), the particles precipitate quickly creating a 'highway' in the middle of the channel, where other particles are dragged in (see frames corresponding to $t = 31, 52$). The sedimentation progresses quite rapidly with all particles settled at time $t = 94$.

On opposite, with $\tau = 1.0$ (long-range repulsion: Fig. 9-bottom), particles maintain a nearly uniform distribution (see frames $t = 31 - 73$) and the resulting sedimentation process is significantly reduced, with most of the particles still settling at $t = 94$. The computational time for these simulations was approximately 40 hrs on 42 Intel X5650 2.67GHz processors at the HPC Wales Cluster.

IV. CONCLUSIONS

In this work we extend the SPH model for the three-dimensional simulation of rigid spherical particles suspended in a viscoelastic matrix. As a fluid model, the coarse-grained SPH viscoelastic formulation proposed in Ref.[37] is used. Property of this particular set of equations is that they are entirely derived within the GENERIC formalism[40] and therefore enjoy automatically thermodynamic consistency. Moreover, the viscoelastic model is derived without reference to a target set of PDEs, but through a microscopic specification of a conformation-tensor-dependent entropy of the fluid particles. In the case of suspended Hookean dumbbells this delivers a particle dynamics which can be interpreted as a specific discretization of the Oldroyd-B constitutive equation.

The deterministic particle model is validated by studying the rotation, migration and dynamics of a single and mutually interacting 'noncolloidal' spheres under confined shear flows. Results are compared against existing numerical data and discussed in terms of available experimental results. Numerical convergence and accuracy of the results as well as influence of interparticle repulsion are discussed in detail.

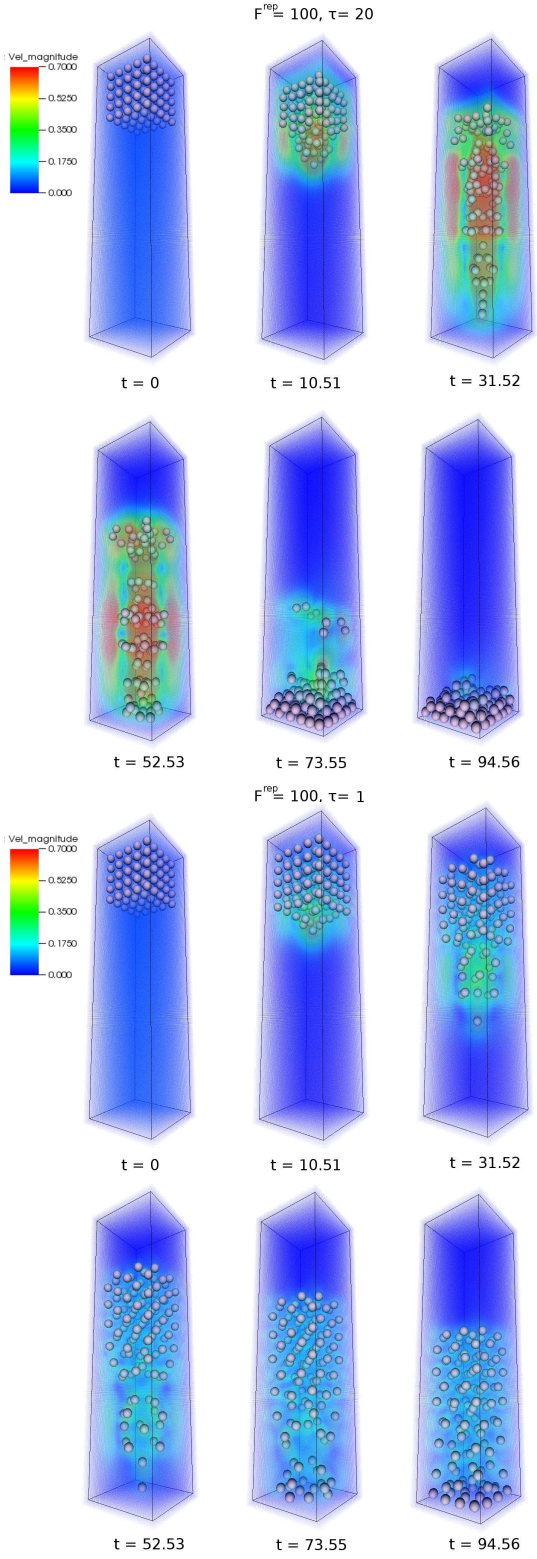

FIG. 9. Sedimentation of particles in a closed cavity at $\mathrm{De} = 0.5$. Interparticle repulsion paramater was $F^{\mathrm{rep}} = 100$, whereas $\tau = 20$ (top: nearly-hard spheres) and $\tau = 1.0$ (bottom: long-range repulsive spheres).

Further possibilities to be explored in the future are the following: (1) modelling 'colloidal' interacting particles in viscoelastic matrices; this can be done straightforwardly in the model presented in[37], by simply switching on the interparticle stochastic terms responsible of Brownian diffusion. The discrete model satisfies exactly the 2nd Law of Thermodynamics and Fluctuation-Dissipation Theorem in virtue of the link to GENERIC. (2) Modelling of more complex viscoelastic fluids could be also explored in the future. This can be done by mesoscopic calculation of the conformation-tensor dependent entropy function for specific dumbbell models, and integrating it into the GENERIC machinery, rather than by brute force top-down SPH discretization of existing continuum models. (3) Finally, we plan to extend the current simulations to a many-particle system in order to study the bulk rheology of complex suspensions.

ACKNOWLEDGMENTS

The authors thank Roger Tanner and Pep Español for very useful discussions. The financial support provided by the Welsh Government and Higher Education Funding Council for Wales through the Ser Cymru National Research Network in Advanced Engineering and Materials is gratefully acknowledged. Computing resources offered by HPC Wales via the Project No. HPCWT050 (Multiscale particle simulation for complex fluids) as well as support from MINECO (Spain) under Grant No. FIS2013-47350-C5-1-R is also gratefully acknowledged.

[1] M. Ahamadi and O. Harlen, "A lagrangian finite element method for simulation of a suspension under planar extensional flow," *Journal of Computational Physics*, vol. 227, no. 16, pp. 7543 – 7560, 2008.

[2] P. Singh, D. Joseph, T. Hesla, R. Glowinski, and T.-W. Pan, "A distributed lagrange multiplier/fictitious domain method for viscoelastic particulate flows," *Journal of Non-Newtonian Fluid Mechanics*, vol. 91, no. 23, pp. 165 – 188, 2000.

[3] N. Patankar, P. Singh, D. Joseph, R. Glowinski, and T.-W. Pan, "A new formulation of the distributed lagrange multiplier/fictitious domain method for particulate flows," *International Journal of Multiphase Flow*, vol. 26, no. 9, pp. 1509 – 1524, 2000.

[4] X. Luo, M. R. Maxey, and G. E. Karniadakis, "Smoothed profile method for particulate flows: Error analysis and simulations," *Journal of Computational Physics*, vol. 228, no. 5, pp. 1750 – 1769, 2009.

[5] S. Padhy, E. Shaqfeh, G. Iaccarino, J. Morris, and N. Tonmukayakul, "Simulations of a sphere sedimenting in a viscoelastic fluid with cross shear flow," *Journal of Non-Newtonian Fluid Mechanics*, vol. 197, pp. 48 – 60, 2013.

[6] J. Brady and G. Bossis, "Stokesian dynamics," *Annual Review of Fluid Mechanics*, vol. 20, no. 1, pp. 111–157, 1988.

[7] A. J. C. Ladd, "Numerical simulations of particulate suspensions via a discretized boltzmann equation. part 1. theoretical foundation," *Journal of Fluid Mechanics*, vol. 271, pp. 285–309, 7 1994.

[8] A. J. C. Ladd and R. Verberg, "Lattice-boltzmann simulations of particle-fluid suspensions," *Journal of Statistical Physics*, vol. 104, no. 5, pp. 1191–1251.

[9] E. S. Boek, P. V. Coveney, H. N. W. Lekkerkerker, and P. van der Schoot, "Simulating the rheology of dense colloidal suspensions using dissipative particle dynamics," *Phys. Rev. E*, vol. 55, pp. 3124–3133, Mar 1997.

[10] M. Whittle and K. P. Travis, "Dynamic simulations of colloids by core-modified dissipative particle dynamics," *The Journal of Chemical Physics*, vol. 132, no. 12, p. 124906, 2010.

[11] N. S. Martys, "Study of a dissipative particle dynamics based approach for modeling suspensions," *Journal of Rheology*, vol. 49, no. 2, pp. 401–424, 2005.

[12] W. Pan, B. Caswell, and G. E. Karniadakis, "Rheology, microstructure and migration in brownian colloidal suspensions," *Langmuir*, vol. 26, no. 1, pp. 133–142, 2010.

[13] S. Jamali, M. Yamanoi, and J. Maia, "Bridging the gap between microstructure and macroscopic behavior of monodisperse and bimodal colloidal suspensions," *Soft Matter*, vol. 9, pp. 1506–1515, 2013.

[14] N. Phan-Thien, N. Mai-Duy, and B. C. Khoo, "A spring model for suspended particles in dissipative particle dynamics," *Journal of Rheology*, vol. 58, no. 4, pp. 839–867, 2014.

[15] X. Bian and M. Ellero, "A splitting integration scheme for the sph simulation of concentrated particle suspensions," *Computer Physics Communications*, vol. 185, no. 1, pp. 53–62, 2014.

[16] A. Vázquez-Quesada and M. Ellero, "Rheology and microstructure of non-colloidal suspensions under shear studied with smoothed particle hydrodynamics," *Journal of Non-Newtonian Fluid Mechanics*, vol. 233, pp. 37–47, 2016.

[17] N. A. Patankar and H. H. Hu, "Rheology of a suspension of particles in viscoelastic fluids," *Journal of Non-Newtonian Fluid Mechanics*, vol. 96, no. 3, pp. 427 – 443, 2001.

[18] Z. Yu, N. Phan-Thien, Y. Fan, and R. I. Tanner, "Viscoelastic mobility problem of a system of particles," *Journal of Non-Newtonian Fluid Mechanics*, vol. 104, no. 23, pp. 87 – 124, 2002.

[19] W. R. Hwang, M. A. Hulsen, and H. E. Meijer, "Direct simulations of particle suspensions in a viscoelastic fluid in sliding bi-periodic frames," *Journal of Non-Newtonian Fluid Mechanics*, vol. 121, no. 1, pp. 15 – 33, 2004.

[20] Y. J. Choi, M. A. Hulsen, and H. E. Meijer, "An extended finite element method for the simulation of particulate viscoelastic flows," *Journal of Non-Newtonian Fluid Mechanics*, vol. 165, no. 1112, pp. 607 – 624, 2010.

[21] G. D'Avino, M. A. Hulsen, F. Snijkers, J. Vermant, F. Greco, and P. L. Maffettone, "Rotation of a sphere in a viscoelastic liquid subjected to shear flow. part i: Simulation results," *Journal of Rheology*, vol. 52, no. 6, pp. 1331–1346, 2008.

[22] G. D'Avino, T. Tuccillo, P. Maffettone, F. Greco, and M. Hulsen, "Numerical simulations of particle migration in a viscoelastic fluid subjected to shear flow," *Computers and Fluids*, vol. 39, no. 4, pp. 709 – 721, 2010.

[23] G. D'Avino, P. Maffettone, F. Greco, and M. Hulsen, "Viscoelasticity-induced migration of a rigid sphere in confined shear flow," *Journal of Non-Newtonian Fluid Mechanics*, vol. 165, no. 910, pp. 466 – 474, 2010.

[24] S. Yoon, M. Walkley, and O. Harlen, "Two particle interactions in a confined viscoelastic fluid under shear," *Journal of Non-Newtonian Fluid Mechanics*, vol. 185186, pp. 39 – 48, 2012.

[25] G. D'Avino, M. A. Hulsen, and P. L. Maffettone, "Separation of particles in non-newtonian fluids flowing in t-shaped microchannels," *Advanced Modeling and Simulation in Engineering Sciences*, vol. 2, no. 1, p. 9, 2015.

[26] N. Jaensson, M. Hulsen, and P. Anderson, "Simulations of the start-up of shear flow of 2d particle suspensions in viscoelastic fluids: Structure formation and rheology," *Journal of Non-Newtonian Fluid Mechanics*, vol. 225, pp. 70 – 85, 2015.

[27] G. D'Avino, F. Greco, M. A. Hulsen, and P. L. Maffettone, "Rheology of viscoelastic suspensions of spheres under small and large amplitude oscillatory shear by numerical simulations," *Journal of Rheology*, vol. 57, no. 3, pp. 813–839, 2013.

[28] S. Krishnan, E. S. Shaqfeh, and G. Iaccarino, "Fully resolved viscoelastic particulate simulations using unstructured grids," *Journal of Computational Physics*, vol. 338, pp. 313 – 338, 2017.

[29] A. Sierou and J. F. Brady, "Accelerated stokesian dynamics sim-

ulations," *Journal of Fluid Mechanics*, vol. 448, pp. 115–146, 12 2001.

[30] H. M. Schaink, J. J. M. Slot, R. J. J. Jongschaap, and J. Mellema, "The rheology of systems containing rigid spheres suspended in both viscous and viscoelastic media, studied by stokesian dynamics simulations," *Journal of Rheology*, vol. 44, no. 3, pp. 473–498, 2000.

[31] Y. K. Lee and K. H. Ahn, "A novel lattice boltzmann method for the dynamics of rigid particles suspended in a viscoelastic medium," *Journal of Non-Newtonian Fluid Mechanics*, vol. 244, pp. 75 – 84, 2017.

[32] A. van den Noort, W. K. den Otter, and W. J. Briels, "Coarse graining of slow variables in dynamic simulations of soft matter," *EPL (Europhysics Letters)*, vol. 80, no. 2, p. 28003, 2007.

[33] I. S. S. de Oliveira, A. van den Noort, J. T. Padding, W. K. den Otter, and W. J. Briels, "Alignment of particles in sheared viscoelastic fluids," *The Journal of Chemical Physics*, vol. 135, no. 10, p. 104902, 2011.

[34] I. S. S. de Oliveira, W. K. den Otter, and W. J. Briels, "The origin of flow-induced alignment of spherical colloids in shear-thinning viscoelastic fluids," *The Journal of Chemical Physics*, vol. 137, no. 20, p. 204908, 2012.

[35] M. Ellero, M. Krger, and S. Hess, "Viscoelastic flows studied by smoothed particle dynamics," *Journal of Non-Newtonian Fluid Mechanics*, vol. 105, no. 1, pp. 35 – 51, 2002.

[36] M. Ellero and R. Tanner, "{SPH} simulations of transient viscoelastic flows at low reynolds number," *Journal of Non-Newtonian Fluid Mechanics*, vol. 132, no. 13, pp. 61 – 72, 2005.

[37] A. Vázquez-Quesada, M. Ellero, and P. Español, "Smoothed particle hydrodynamic model for viscoelastic fluids with thermal fluctuations," *Physical Review E*, vol. 79, no. 5, p. 056707, 2009.

[38] A. Vázquez-Quesada, M. Ellero, and P. Español, "A sph-based particle model for computational microrheology," *Microfluidics and nanofluidics*, vol. 13, no. 2, pp. 249–260, 2012.

[39] H. C. Ottinger, *Complex Fluids*, pp. 97–156. John Wiley Sons, Inc., 2005.

[40] M. Grmela and H. C. Öttinger, "Dynamics and thermodynamics of complex fluids. i. development of a general formalism," *Phys. Rev. E*, vol. 56, pp. 6620–6632, Dec 1997.

[41] A. Vázquez-Quesada and M. Ellero, "Sph simulations of a viscoelastic flow around a periodic array of cylinders confined in a channel," *Journal of Non-Newtonian Fluid Mechanics*, vol. 167, pp. 1–8, 2012.

[42] M. Grilli, A. Vázquez-Quesada, and M. Ellero, "Transition to turbulence and mixing in a viscoelastic fluid flowing inside a channel with a periodic array of cylindrical obstacles," *Physical review letters*, vol. 110, no. 17, p. 174501, 2013.

[43] I. Sbalzarini, J. Walther, M. Bergdorf, S. Hieber, E. Kotsalis, and P. Koumoutsakos, "Ppm - a highly efficient parallel particlemesh library for the simulation of continuum systems," *Journal of Computational Physics*, vol. 215, no. 2, pp. 566 – 588, 2006.

[44] J. P. Morris, P. J. Fox, and Y. Zhu, "Modeling low reynolds number incompressible flows using sph," *Journal of computational physics*, vol. 136, no. 1, pp. 214–226, 1997.

[45] M. Ellero and N. A. Adams, "Sph simulations of flow around a periodic array of cylinders confined in a channel," *International Journal for Numerical Methods in Engineering*, vol. 86, no. 8, pp. 1027–1040, 2011.

[46] X. Bian, S. Litvinov, R. Qian, M. Ellero, and N. A. Adams, "Multiscale modeling of particle in suspension with smoothed dissipative particle dynamics," *Physics of Fluids*, vol. 24, no. 1, p. 012002, 2012.

[47] A. Vázquez-Quesada, X. Bian, and M. Ellero, "Three-dimensional simulations of dilute and concentrated suspensions using smoothed particle hydrodynamics," *Computational Particle Mechanics*, vol. 3, no. 2, pp. 167–178, 2016.

[48] S. Kim and S. J. Karrila, *Microhydrodynamics: principles and selected applications*. 1991.

[49] S. Litvinov, M. Ellero, X. Hu, and N. Adams, "A splitting scheme for highly dissipative smoothed particle dynamics," *Journal of Computational Physics*, vol. 229, no. 15, pp. 5457–5464, 2010.

[50] G. Karniadakis, A. Beskok, and N. Aluru, "Microflows and nanoflows: Fundamentals and simulation (interdisciplinary applied mathematics, 29)," p. 824.

[51] R. I. Tanner and S. Dai, "Rheology of non-colloidal suspensions with corn syrup matrices," *Rheologica Acta*, vol. 55, no. 9, pp. 739–747, 2016.

[52] D. Dratler and W. Schowalter, "Dynamic simulation of suspensions of non-brownian hard spheres," *Journal of Fluid Mechanics*, vol. 325, pp. 53–77, 1996.

[53] J. F. Brady and J. F. Morris, "Microstructure of strongly sheared suspensions and its impact on rheology and diffusion," *Journal of Fluid Mechanics*, vol. 348, pp. 103–139, 1997.

[54] F. Snijkers, G. D'Avino, P. L. Maffettone, F. Greco, M. Hulsen, and J. Vermant, "Effect of viscoelasticity on the rotation of a sphere in shear flow," *Journal of Non-Newtonian Fluid Mechanics*, vol. 166, no. 7, pp. 363–372, 2011.

[55] F. Snijkers, G. D'Avino, P. L. Maffettone, F. Greco, M. Hulsen, and J. Vermant, "Rotation of a sphere in a viscoelastic liquid subjected to shear flow. part ii. experimental results," *Journal of Rheology*, vol. 53, no. 2, pp. 459–480, 2009.

[56] P. Y. Huang, J. Feng, H. H. Hu, and D. D. Joseph, "Direct simulation of the motion of solid particles in couette and poiseuille flows of viscoelastic fluids," *Journal of Fluid Mechanics*, vol. 343, p. 7394, 1997.

[57] S. Caserta, G. D'Avino, F. Greco, S. Guido, and P. L. Maffettone, "Migration of a sphere in a viscoelastic fluid under planar shear flow: Experiments and numerical predictions," *Soft Matter*, vol. 7, pp. 1100–1106, 2011.

[58] B. P. Ho and L. G. Leal, "Inertial migration of rigid spheres in two-dimensional unidirectional flows," *Journal of Fluid Mechanics*, vol. 65, no. 2, p. 365400, 1974.

[59] G. D'Avino and P. Maffettone, "Particle dynamics in viscoelastic liquids," *Journal of Non-Newtonian Fluid Mechanics*, vol. 215, pp. 80 – 104, 2015.

[60] G. Batchelor and J.-T. Green, "The hydrodynamic interaction of two small freely-moving spheres in a linear flow field," *Journal of Fluid Mechanics*, vol. 56, no. 02, pp. 375–400, 1972.

[61] F. Snijkers, R. Pasquino, and J. Vermant, "Hydrodynamic interactions between two equally sized spheres in viscoelastic fluids in shear flow," *Langmuir*, vol. 29, no. 19, pp. 5701–5713, 2013. PMID: 23600865.